Ensemble Kalman Update for Inference of Spatial Uniformity of Emission across an Electrospray Array

Ensemble Kalman Update for Inference of Spatial Uniformity of Emission across an Electrospray Array

Oliver Jia-Richards and Paulo C. Lozano
Space Propulsion Laboratory
Massachusetts Institute of Technology
Cambridge, MA, 02139
{oliverjr, plozano}@mit.edu

***Abstract*—The spatial uniformity of emission across an electrospray thruster array can impact several performance characteristics of the thruster such as the thrust vector and overall thruster lifetime. For example, spatial variation of emission across an array could lead to variations of the center of thrust of the thruster which can induce undesired disturbance torques on the spacecraft. However, the small size of many electrospray thruster arrays means that most of the performance characteristics are determined on a global scale since emitter-to-emitter performance variations cannot be directly measured. The ability to determine emitter-to-emitter variations could greatly increase our understanding of how such thrusters operate as well as inform the design of future thrusters. Previous methods to determine the spatial uniformity of emission have led to the ability to visualize the spatial distribution in a qualitative manner, but cannot provide quantitative emission characteristics at the individual emitter scale. This work explores the use of the ensemble Kalman update, a form of approximate Bayesian inference, in order to infer individual emitter emission properties based on measurements of the emitted current density taken downstream of the array. The use of an inference method alleviates the issue of attempting to directly measure the emission properties of individual emitters and could simplify the required measurement setups in order to determine spatial uniformity of emission. The efficacy of this method is demonstrated on simulated data for a 300-emitter circular array with point measurements of the current density, but is easily extendable to other array geometries and measurement systems. Uncertainty in the angular distribution of the emitted ion beam is also discussed and incorporated.**

TABLE OF CONTENTS

1. INTRODUCTION

The design of electrospray thrusters typically involves the multiplexing of multiple electrospray emitters. Such a design allows for a large amount of flexibility in thruster architecture; some thrusters use as few as 9 emitters [1] while other thrusters use 10s of emitters [2] or even 100s of emitters [3]. However, performance characteristics for electrospray thrusters are typically measured on a macroscopic scale and consider the combined contribution of all of the emitters on the thruster. Quite often the performance of individual emitters on the array is not considered. This is in part due to the macroscopic performance characteristics such as thrust and specific impulse being more important for applications of the thruster to various missions, but also due to the difficulty of measuring the performance characteristics of individual emitters. In thrusters designed for small spacecraft, the distance between neighboring emitters can be on the order of 100 μm. Direct measurements of individual emitters would require that measurements be taken on the order of 100 μm away from the thruster face.

The performance characteristics of individual emitters can have impacts on the performance of the thruster as a whole. Impingement between individual emitters and the extractor grid can influence the lifetime of the thruster [4] as well as the characteristics of spacecraft charging [5]. In addition, non-uniformity in spatial distribution of emission could lead to uncertainty in the thrust vector both in terms of center and direction. It is typically assumed that the thrust vector is centered on the thruster with direction perpendicular to the thruster face, but this is likely not true in practice. Deviations of both the thrust center as well as thrust vector direction could lead to undesired disturbance torques on the spacecraft. While the magnitude of the torque will be relatively small, since the torque would act over an extended period of time it could have a significant effect on the spacecraft's momentum management system.

Various attempts have been made in order to probe the spatial uniformity of emission across an electrospray array. A scanning current probe was used to obtain measurements approximately 200 μm from the thruster face [6]. Such an approach could allow for direct measurement of individual emitter properties, but the proximity of the probe to the emission sites can influence the emitters' emission characteristics so only qualitative conclusions were possible. Computed tomography has been used to obtain measurements 2 mm [7] and 4 mm [8] away from the thruster face which reduces the influence of the probe on the emission characteristics, but only provides a qualitative assessment since the emitted ion beams from neighboring emitters will overlap at such distances. Finally, an optical system was considered in order to capture the faint light emitted during ion emission [9]. Again, only a qualitative assessment of the uniformity of emission across the thruster can be made from such a system.

In order to provide a more-detailed assessment of the spatial uniformity of emission across an electrospray array, an approach that can provide a quantitative assessment of the emission characteristics for individual emitters is required. In particular, analyzing the center of thrust will require knowledge of the current output for each emitter. In lieu of taking direct measurements, this work proposes the use of Bayesian inference in order to determine quantitative results. Given a vector of parameters ψ and a prior probability of the parameter vector $\mathcal{P}(\psi)$, then the goal of Bayesian inference

is to update the probability of the parameter vector based on a vector of observed measurements y. This posterior probability is related to the prior probability through

$$\mathcal{P}(\psi|y) \propto \mathcal{P}(y|\psi)\mathcal{P}(\psi) \tag{1}$$

where $\mathcal{P}(y|\psi)$ is the likelihood of observing the measurements given a particular parameter vector. For an electrospray thruster a simple parameter vector may be the current emitted by each emitter and the measurement vector may be the current density measured downstream of the thruster using a measurement system similar to those in Refs. [6] or [8]. Given a model that can simulate the measurements for a particular parameter vector, various algorithms exist in order to generate samples whose distribution matches or approximates the posterior probability.

The purpose of this paper is to demonstrate the efficacy of the ensemble Kalman update as a means of approximating the posterior probability. The ensemble Kalman update is a relatively simple algorithm that can be adapted to a wide variety of model parameterizations or measurement schemes. In addition, the incorporation of model uncertainty is much simpler than for other algorithms that may provide an exact solution for the posterior probability such as Markov Chain Monte Carlo. Section 2 provides an overview of the ensemble Kalman update algorithm. Section 3 discusses the specific implementation details for using the ensemble Kalman update to infer the current of individual emitters on an electrospray thruster based on downstream current density measurements. In this work the parameter vector only consists of the current emitted by each emitter and the measurement scheme is similar to that of Ref. [6]. Section 4 provides an example based on simulated data for a 300-emitter circular thruster and Section 5 summarizes the results.

2. ALGORITHM

The ensemble Kalman update [10] is a form of approximate Bayesian inference meaning that the distribution of samples it generates approximates the true posterior distribution. The idea behind the ensemble Kalman update is the same as the update step of a standard Kalman filter where parameters of inference are updated based on a linear update rule

$$\psi = \psi - K(y - y^*) \tag{2}$$

where K is the Kalman gain, y is the vector of simulated measurements based on the current estimate of the parameters, and y^* is the vector of observed measurements. For linear-Gaussian models, the Kalman gain can be calculated analytically based on the measurement model and prior uncertainty in the parameters. However, for models that contain nonlinearities or non-Gaussian distributions an analytical form of the Kalman gain is generally not possible to obtain.

Instead, the ensemble Kalman update attempts to approximate the Kalman gain through Monte Carlo methods. The key idea is that the Kalman gain can be calculated from

$$K = \Sigma_{\psi,y}\Sigma_y^{-1} \tag{3}$$

where $\Sigma_{\psi,y}$ is the covariance between the parameters and measurements, and Σ_y is the auto-covariance of the measurements. By generating an ensemble of initial parameter estimates, based on the assumed prior distribution of the parameters, the measurements for each ensemble member can be simulated from a model of the system. With a collection of parameter estimates and corresponding measurements, $\Sigma_{\psi,y}$ and Σ_y can be numerically estimated which allows for an estimate of the Kalman gain to be obtained.

Algorithm 1 shows the ensemble Kalman update routine. The ensemble, Ψ, consists of a collection of parameter vectors. For a given number of ensemble members, each member of the ensemble is generated by randomly sampling a parameter vector from the prior distribution, $\mathcal{P}(\psi)$. Then, a model of the system, $f(\psi)$, is used to generate a simulated measurement vector given the parameter vector for each ensemble member. Given the collection of parameter vectors and simulated measurement vectors, the covariances $\Sigma_{\psi,y}$ and Σ_y are estimated which allows a numerical estimate of the Kalman gain to be obtained. With the estimate of the Kalman gain, the parameter estimates for each ensemble member can be updated using the linear update rule in Eq. 2. The posterior distribution of the parameter vectors in the ensemble is then an approximation of the true posterior distribution in Eq. 1.

Algorithm 1 Ensemble Kalman update

1: Given observed measurement vector, y^*
2: Initialize ensemble, Ψ
3: Initialize measurement matrix, Υ
4: **for** each ensemble member i **do**
5: Draw parameter vector from prior, $\Psi_i \leftarrow \mathcal{P}(\psi)$
6: Simulate measurement vector, $\Upsilon_i = f(\Psi_i)$
7: Estimate $\Sigma_{\psi,y}$ and Σ_y from Ψ and Υ
8: Estimate Kalman gain, $K = \Sigma_{\psi,y}\Sigma_y^{-1}$
9: **for** each ensemble member i **do**
10: Update parameter vector, $\Psi_i = \Psi_i - K(\Upsilon_i - y^*)$
11: **return** ensemble, Ψ

3. IMPLEMENTATION

In order to implement the ensemble Kalman update, a model that simulates measurements given a particular set of parameter settings is required. For this work, the parameters of interest are the current emitted by each emitter and the measurements are measurements of the current density downstream of the array. Under the assumption that the beams of neighboring emitters do not interact, the system model is a superposition of the current density from each emitter on the array at each measurement point. Therefore, the model for a full electrospray thruster array is based on the model for a single emitter that relates the emitted current to the measured current density at any point downstream.

Models of the emitted ion beam from an electrospray emitter are typically defined by their angular distribution. Multiple profile shapes for the angular distribution of current density downstream of an electrospray emitter have been proposed, such a parabolic profile [11]. In this work an exponential power profile is used

$$g(\theta, L, p) = \exp\left[-\frac{1}{p}\left(\frac{\theta}{L}\right)^p\right] \tag{4}$$

which, in a slightly different form, is also referred to as a super-Gaussian profile [12]. θ is the angle measured away from the center of the beam, L controls the length scale of the profile, and p controls its sharpness. A form of this exponential power profile with $p = 2$ is commonly used as a kernel for Gaussian processes and motivated its application here. Figure 1 shows example profiles. As p increases, the

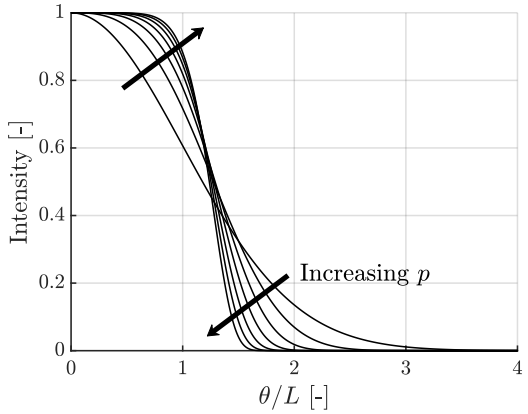

Figure 1. Example profiles of the current density intensity versus θ/L for different values of p.

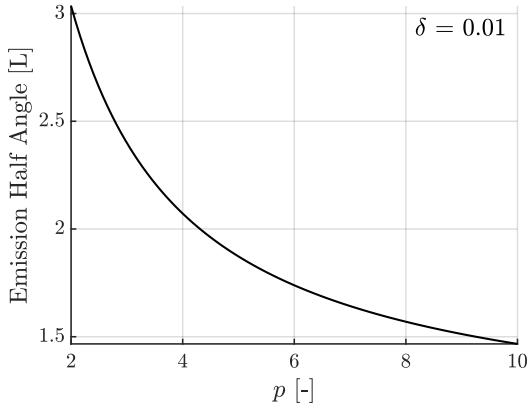

Figure 2. Approximate half angle of the emitted ion beam in terms of the profile parameter L for different values of p based on $\delta = 0.01$.

center of the profile becomes flatter and there is a steeper drop off in intensity.

A notable aspect of the exponential power profile is that the value of the function never reaches zero. Therefore, the half angle of emission for an ion beam is defined here as the angle at which the intensity of the current density drops below some fraction δ of the intensity at the center of the beam. This amounts to solving

$$\exp\left[-\frac{1}{p}\left(\frac{\hat{\theta}}{L}\right)^p\right] = \delta \tag{5}$$

which gives the half angle of emission normalized by the length scale of the profile, L, as

$$\frac{\hat{\theta}}{L} = \left[p \ln\left(\frac{1}{\delta}\right)\right]^{1/p} \tag{6}$$

Figure 2 shows the normalized half angle of emission for different values of p assuming δ = 0.01. Typical values of p for an electrospray beam fall in the range (3, 5) indicating that the half angle of emission will be approximately $2L$, but can approach $3L$ for $p \approx 2$.

With the exponential power profile, the current density is

$$j(\theta, R, L, p, I_{\text{emitter}}) = \frac{1}{n(R, L, p)} \exp\left[-\frac{1}{p}\left(\frac{\theta}{L}\right)^p\right] I_{\text{emitter}} \tag{7}$$

where I_{emitter} is the current of the emitter, $n(R, L, p)$ is a normalization factor in order to ensure that the current density integrates to the emitter current over a surface surrounding the emitter tip, and R is the distance from the emitter tip to the measurement location. Assuming that the emitter does not fire backwards, the surface can be taken to be a hemisphere of radius R with the emitter at the center. The normalization factor can then be calculated from

$$n(R, L, p) = 2\pi R^2 \int_0^{\pi/2} \exp\left[-\frac{1}{p}\left(\frac{\theta}{L}\right)^p\right] \sin(\theta)\, d\theta \tag{8}$$

which unfortunately does not have an analytical solution. Two approximations are made in order to obtain an analytical approximation for the normalization factor. First, a three-term Taylor series expansion for $\sin(\theta)$ is used

$$\sin(\theta) \approx \theta - \frac{\theta^3}{3!} + \frac{\theta^5}{5!} \tag{9}$$

which has error less than 0.5% for $0 \leq \theta \leq \pi/2$. Second, the limit of the integration is extended to infinity. As long as the half angle of emission is less than $\pi/2$ then the value of the integrand is near-zero for $\theta > \pi/2$. Therefore, extending the upper limit of the integration to infinity will not have an appreciable effect on the integral value, but does simplify the final result. With these two approximations, an analytical approximation for the normalization factor can be obtained

$$n(R, L, p) \approx 2\pi R^2 \left[L^2 p^{-1+\frac{2}{p}} \Gamma\left(\frac{2}{p}\right) - \frac{1}{6} L^4 p^{-1+\frac{4}{p}} \Gamma\left(\frac{4}{p}\right) + \frac{1}{120} L^6 p^{-1+\frac{6}{p}} \Gamma\left(\frac{6}{p}\right)\right] \tag{10}$$

where Γ is the gamma function

$$\Gamma(z) = \int_0^\infty x^{z-1} \exp(-x) dx \tag{11}$$

Figure 3 shows an exponential power profile fit to experimental data for a single electrospray emitter from Ref. [13] by combining the data for both positive and negative polarity emission at a current of approximately 200 nA. The dashed lines show the 95% confidence interval of the profile fit. Table 1 shows the mean and standard deviation for the profile parameters and Figure 4 shows the resulting distribution of the emission half angle for δ = 0.01. Due to the low number of experimental data points the uncertainty in the profile fit is quite large, and the resulting uncertainty in emission half angle covers a range of approximately 10 degrees. However, all estimates of the emission half angle are much lower than 90 degrees, indicating that the approximations used to generate Eq. 10 are valid.

For implementation, it is desirable to incorporate the uncertainty in the angular distribution profile fit into the system model. Each call to the model generates a random value of L and p for each emitter based on the parameters in Table 1

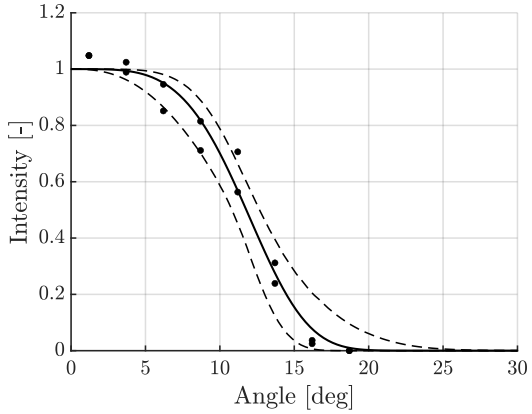

Figure 3. Measurements of the current density versus angle along with exponential power function fit. Dashed lines show 95% confidence interval of the fit.

Table 1. Mean and standard deviation of exponential power function parameters when fit to experimental data.

	Mean	Standard Deviation	Unit
L	9.1259	0.2737	deg
p	4.0930	0.5879	

and assuming a Gaussian distribution for each parameter. By incorporating the model uncertainty in this way the system model is stochastic, and the variance of the measurements will be influenced by both the measurement noise and the model uncertainty.

Algorithm 2 shows the system model under the assumption that the measurements are point measurements of the current density at various locations. Other measurement models such as the computed tomography technique of Refs. [7] and [8] are possible, and just require a modification to the calculation of the measurement vector to be used. Given a parameter vector, which in this work consists of the current of each emitter on the array, the measurement vector is computed by superimposing the contribution of each emitter to each measurement. An outer loop iterates through each emitter and draws random parameters for the exponential power profile based on the parameters in Table 1. An inner loop iterates through each measurement and adds the contribution of the emitter to the overall measurement. Finally, measurement noise is added to each measurement. In this work, the measurement noise is assumed to be Gaussian with standard deviation equal to some fraction λ of the measurement magnitude. Unless otherwise specified, $\lambda = 0.01$.

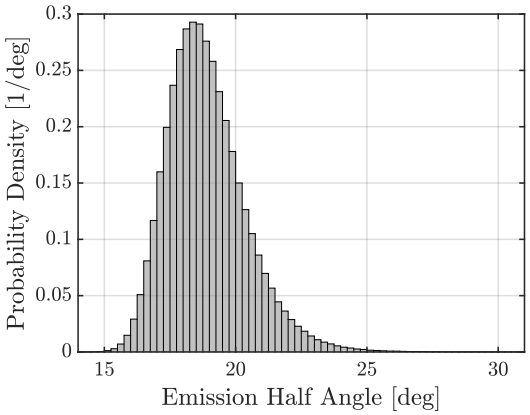

Figure 4. Probability density of the approximate half angle of the emitted ion beam based on $\delta = 0.01$.

Algorithm 2 System model

Given parameter vector, ψ
Initialize measurement vector, y
for each emitter i **do**
  Draw profile length scale, $L_i \leftarrow \mathcal{N}(\mu_L, \sigma_L)$
  Draw profile sharpness, $p_i \leftarrow \mathcal{N}(\mu_p, \sigma_p)$
  for each measurement k **do**
    Calculate emitter to measurement angle, $\theta_{i,k}$
    Calculate emitter to measurement distance, $R_{i,k}$
    Calculate current density from Eq. 7,
      $j_{i,k} = j(\theta_{i,k}, R_{i,k}, L_i, p_i, \psi_i)$
    Increment measurement, $y_k = y_k + j_{i,k}$
for each measurement k **do**
  Draw measurement noise, $\tilde{y}_k \leftarrow \mathcal{N}(0, \lambda y_k)$
  Add measurement noise, $y_k = y_k + \tilde{y}_k$
return measurement vector, y

The final aspect of the implementation is the prior distribution of the parameter vector, $\mathcal{P}(\psi)$. Since the parameter vector here consists of the current of each emitter, the prior distribution is controlled by the assumed distribution of current for an electrospray emitter. For this work it is assumed that the current of each emitter is drawn independently from a uniform distribution that ranges from 0 nA to 600 nA. Other prior distributions for the emitter currents can be used both in terms of distribution shape as well as incorporating any correlation between the currents of neighboring emitters.

4. EXAMPLE

For an example, a 300-emitter circular thruster with diameter of 1 cm is considered. Emitters are arranged in a sunflower arrangement [14] in order to achieve roughly even spacing of the emitters. Measurements are assumed to be taken in a plane parallel to, but offset from, the thruster face. The measurement pattern considered here is a 101 x 101 square grid pattern centered over the thruster and with side length slightly larger than the thruster diameter in order to capture spreading of the ion beams. This measurement pattern is similar to the measurements taken in Ref. [6]. Figure 5 shows the emitter and measurement locations in the x-y plane with both axes normalized by the thruster diameter. For this thruster and measurement pattern, the spacing between neighboring emitters is approximately 500 μm and the spacing between neighboring measurements is 250 μm.

Figure 6 shows the true emitter currents used to simulate the observed measurements. The current of each emitter is assumed to be drawn from a uniform distribution ranging from 0 nA to 600 nA. A correlation between neighboring emitter currents of approximately 0.1 the thruster diameter is intentionally introduced in order to generate "hot" and "cold" spots on the emitter. This correlation is only included when generating the true emitter currents and is not included in the prior distribution used during inference.

Simulated scans of the current density measurements at distances of 1-4 mm away from the thruster face are shown in Figure 7. At 1 mm individual emitters are still discernible;

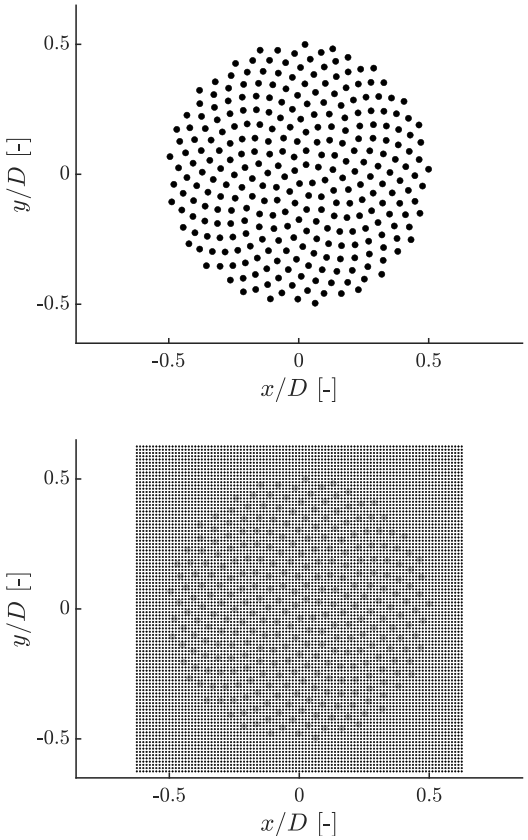

Figure 5. Locations of emitters (top) and measurements (bottom) in the x-y plane.

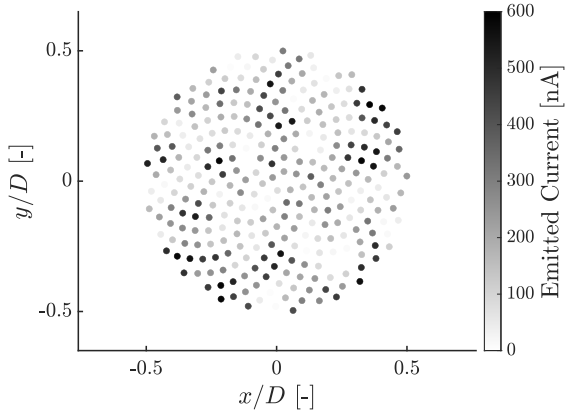

Figure 6. True values of the emitted current for each emitter on the array.

while the emitter beams do overlap at this distance, they only overlap in the tails of their angular distributions. As the distance between the measurement plane and thruster face increases, the ion beams overlap more and more and the measurements become blurry. At 2 mm individual emitters are still somewhat visible, but at 3 mm and 4 mm individual emitters cannot be seen and only clumps of "hot" and "cold" spots on the thruster face are observable. While the ensemble Kalman update can be used for any measurement distance, its performance will improve the closer measurements are taken to the thruster face as changes to the current emitted by different emitters will have a larger influence on the measurements. However, taking measurements closer to the thruster face requires a more precise measurement system and can lead to concerns regarding the probe used for taking measurements interfering with the ion beams and altering the measurements. For this work a measurement distance of 2 mm is used for detailed study to match the measurement distance of Ref. [7].

The mean of the inferred values of the emitter currents based on measurements taken 2 mm away from the thruster face are shown in Figure 8. For inference, 500,000 ensemble members were used which provides 500,000 estimates for each current value. Qualitatively, the results look quite similar to the true values in Figure 6. Figure 9 shows the error between the mean of the inferred values of the emitter currents and their true values. The inferred values of all emitter currents are accurate to within $\pm$30 nA and most values are accurate to within $\pm$10 nA. Figure 10 shows the standard deviation of the inferred values of all emitter currents. Most emitters have a standard deviation of their inferred value of approximately 10 nA. However, Figure 10 shows a clear trend where the inferred values of current for emitters towards the edge of the thruster have lower standard deviation relative to those for emitters towards the center of the thruster. Figure 11 shows the standard deviation of the inferred values of emitter currents versus the radial position of the emitter. The standard deviation is relatively constant towards the center of the thruster, but there is a sharp decrease in standard deviation towards the edge of the thruster. The emitters on the very edge of the thruster are notably separated, and have relatively low standard deviation for their inferred current values. Finally, Figure 12 shows the error between the mean of the inferred values of the emitter currents and their true values normalized by the standard deviation of each inferred value. The error for each mean value falls within three standard deviations of the true value in all cases.

Figure 13 shows the effect of measurement distance on the standard deviation of inferred values for the inner emitters: those with radial position less than half the radius of the thruster. The marker shows the average value while the error bars show the full range of data. Estimates of emitter currents precise to a few nano-Amps could be achieved at a measurement distance of 1 mm. Measurements taken at 3 mm sacrifice estimate accuracy and precision, but may simplify the required measurement setup.

5. CONCLUSION

This work shows that the ensemble Kalman update could be used to infer individual emitter properties based on downstream measurements of the current density. For a thruster with emitter-to-emitter spacing of around 500 μm, estimate accuracies of within 30 nA were achievable for measurements taken 2 mm from the thruster face. While these results are

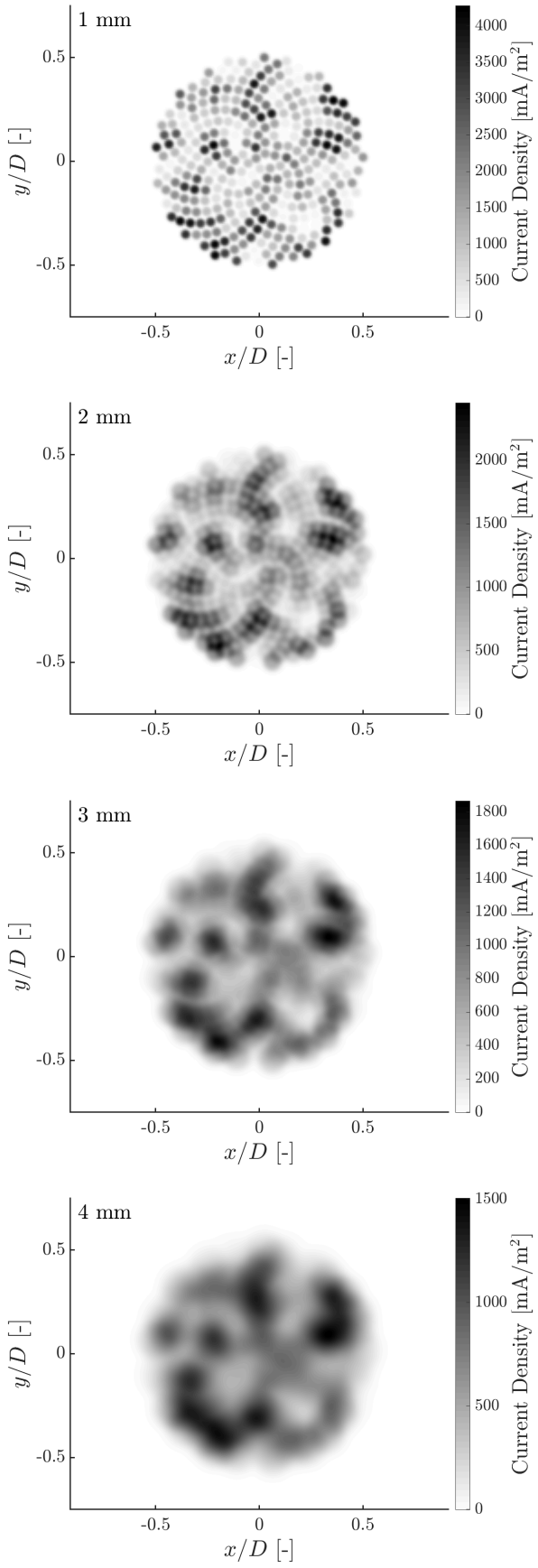

Figure 7. Simulated scans of current density measured at 1-4 mm away from the thruster face.

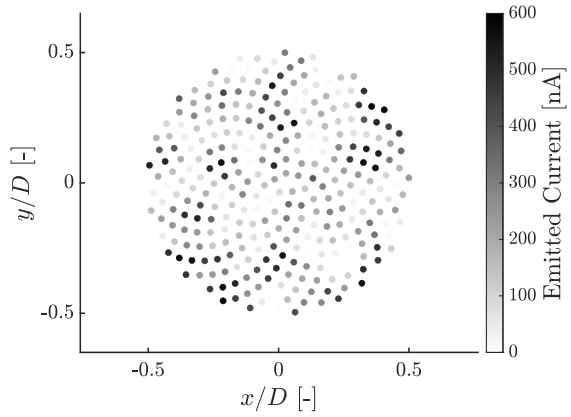

Figure 8. Mean of the inferred values of the emitted current for each emitter on the array.

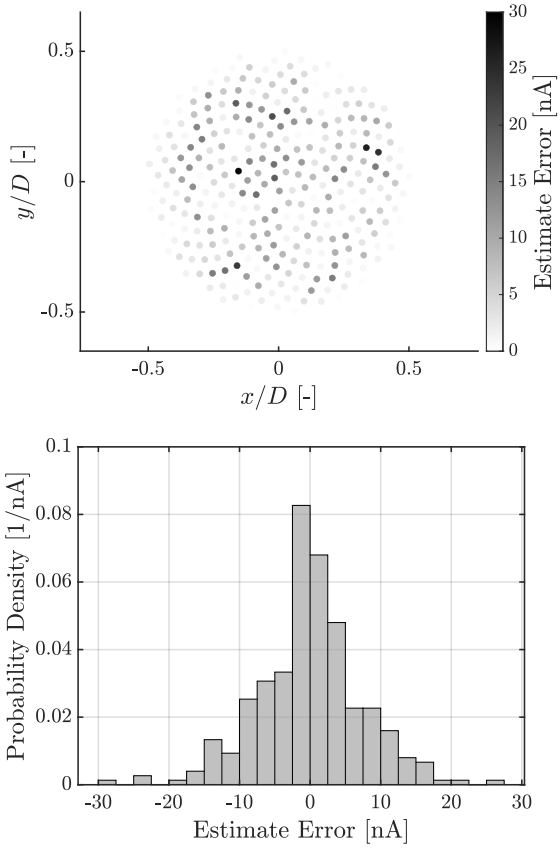

Figure 9. Error between the mean of the inferred values of the emitted current and the true values for a measurement distance of 2 mm.

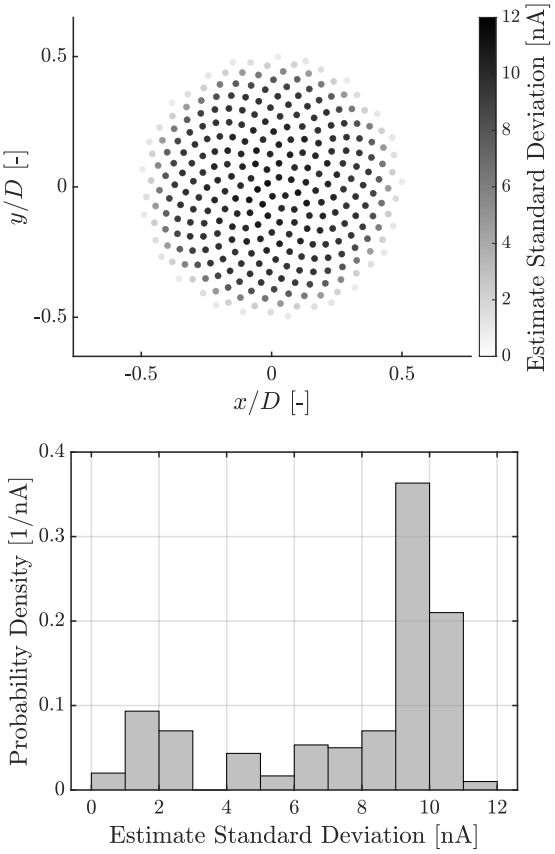

Figure 10. Standard deviation of the inferred values of the emitted current for a measurement distance of 2 mm.

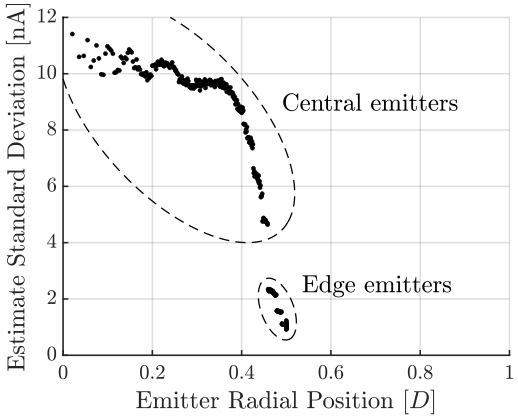

Figure 11. Standard deviation of the inferred values of the emitted current for a measurement distance of 2 mm versus radial position of the emitter.

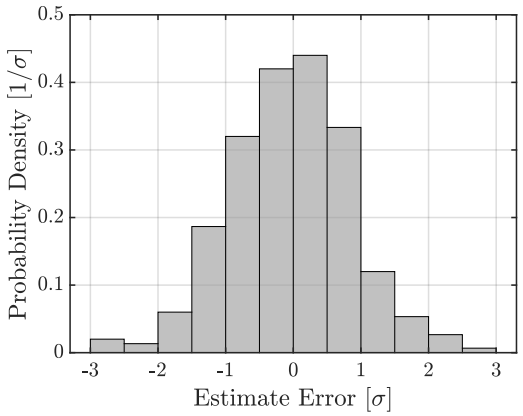

Figure 12. Error between the mean of the inferred values of the emitted current and the true values normalized by the standard deviation of each inferred value.

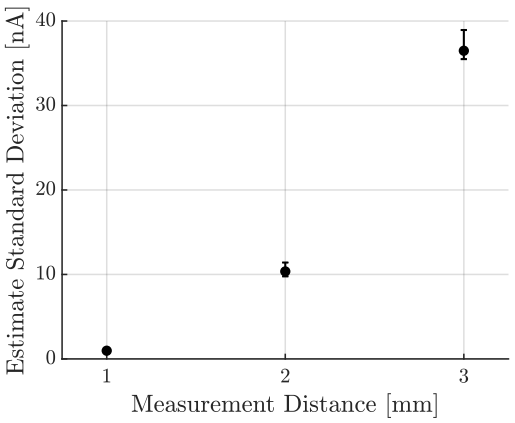

Figure 13. Standard deviation of the inferred values of current for the inner emitters versus measurement distance.

specific to the thruster and measurement scheme used here, it is likely that thrusters with similar emitter and measurement spacings will see uncertainty of a similar magnitude.

The parameter vector in this work only contained the current emitted by each emitter. The parameter vector and system model can be expanded to account for other effects such as off-axis firing or blocked emission due to impingement with the extractor grid. It is also possible that the approach can be applied to linear emitters with a variable number of emission sites such as those in Ref. [15] assuming an appropriate parameterization of the emission is provided. The ensemble Kalman update approach can be further improved by enhanced modeling of emission from an electrospray thruster. Both interactions between the ion beams of neighboring emitters as well as uncertainties in the angular distribution profile will result in a better assessment of the uncertainty in the inferred current. In this work the uncertainty in the angular distribution profile was determined based on limited experimental data taken at a single operating point. Dedicated experimental work will likely be required in order to properly assess the true uncertainty in the angular distribution profile, including how the profile parameters change for different operating points and measurement distances.

REFERENCES

[1] J. Ziemer *et al.*, "In-Flight Verification and Validation of Colloid Microthruster Performance." Cincinnati, OH: AIAA Propulsion and Energy Forum, July 2018.

[2] D. Krejci *et al.*, "Full Performance Mapping of the IFM Nano Thruster, Including Direct Thrust Measurements," *Journal of Small Satellites*, vol. 8, no. 2, pp. 881–893, 2019.

[3] E. Petro, A. Bruno, P. Lozano, L. Perna, and D. Freeman, "Characterization of the TILE Electrospray Emitters." Virtual Event: AIAA Propulsion and Energy Forum, August 2020.

[4] A. Thuppul, P. Wright, A. Collins, J. Ziemer, and R. Wirz, "Lifetime Considerations for Electrospray Thrusters," *Aerospace*, vol. 7, no. 8, p. 108, 2020.

[5] F. Mier-Hicks and P. Lozano, "Spacecraft-Charging Characteristics Induced by the Operation of Electrospray Thrusters," *Journal of Propulsion and Power*, vol. 33, no. 2, pp. 456–467, 2017.

[6] C. Guerra-Garcia, D. Krejci, and P. C. Lozano, "Spatial Uniformity of the Current Emitted by an Array of Passively Fed Electrospray Porous Emitters," *Journal of Physics D: Applied Physics*, vol. 49, no. 11, p. 115503, 2016.

[7] T. Fedkiw, Z. Wood, and N. Demmons, "Improved Computed Tomography Current Mapping of Electrospray Thrusters." Virtual Event: AIAA Propulsion and Energy Forum, August 2021.

[8] D. Courtney, Z. Wood, and T. Fedkiw, "Reconstructing Electrospray Plume Current Spatial Distributions using Computed Tomography." University of Vienna, Austria: 36th International Electric Propulsion Conference, September 2019.

[9] C. Chen, M. Chen, W. Fan, and H. Zhou, "Effects of Non-Uniform Operation of Emission Sites on Characteristics of a Porous Electrospray Thruster," *Acta Astronautica*, vol. 178, pp. 192–202, 2021.

[10] G. Evensen, "The Ensemble Kalman Filter: Theoretical Formulation and Practical Implementation," *Ocean Dynamics*, vol. 52, pp. 343–367, 2003.

[11] C. Perez-Martinez, S. Guilet, J. Gierak, and P. Lozano, "Ionic Liquid Ion Sources as a Unique and Versatile Option in FIB Applications," *Microelectronic Engineering*, vol. 88, no. 8, pp. 2088–2091, 2011.

[12] A. Thuppul, A. Collins, P. Wright, N. Uchizono, and R. Wirz, "Mass Flux and Current Density Distributions of Electrospray Plumes," *Journal of Applied Physics*, vol. 130, no. 10, p. 103301, 2021.

[13] P. Lozano and M. Martínez-Sánchez, "Ionic Liquid Ion Sources: Characterization of Externally Wetted Emitters," *Journal of Colloid and Interface Science*, vol. 282, no. 2, pp. 415–421, 2005.

[14] H. Vogel, *Mathematical Biosciences*, vol. 44, no. 3–4, pp. 179–189, 1979.

[15] T. Fedkiw, Z. Wood, and N. Demmons, "Environmental and Lifetime Testing of the BET-300-P Electrospray Thruster." Virtual Event: AIAA Propulsion and Energy Forum, August 2020.

ACKNOWLEDGMENTS

The authors would like to thank Youssef Marzouk for his assistance with this work. Funding was provided by a NASA Space Technology Research Fellowship under grant 80NSSC18K1186. In addition, Paulo Lozano would like to thank the Miguel Alemán-Velasco foundation for its support.

BIOGRAPHY

Oliver Jia-Richards *is a Doctoral Candidate and NASA Space Technology Research Fellow in the Space Propulsion Laboratory at MIT. He earned his S.B. and S.M. in aeronautical and astronautical engineering from MIT. His current research focuses on the use of electrospray thrusters for the exploration of planetary bodies ranging from small asteroids to planets.*

Paulo C. Lozano *is the Miguel Alemán-Velasco Professor of Aeronautics and Astronautics at MIT and the director of the Space Propulsion Laboratory. He earned his S.M. and Ph.D. in space propulsion from MIT. His research features the development of highly efficient and compact ion thrusters for applications in space systems, including pico- and nano-satellites.*